the addition of substrate, less than 5% of the radioactivity remained as unesterified fatty acid. These results indicate that the fatty acids were taken up by the cells and used in the cellular reactions of lipid synthesis. However, 24 hours after the start of the experiments, 96 to 98% of the radioactivity was recovered as the original fatty acid supplied and no label could be detected in DHA or DPA.

26. mRNA was isolated from PUFA-producing *Schizochytrium* (American Type Culture Collection number 20888) cells grown in a fermentor, and a cDNA library was produced with the GIBCO BRL Superscript Plasmid Cloning System with vector pSPORT1. Clones were randomly chosen and sequenced from the 5′ end with a universal sequencing primer.
27. Supplementary material is available on *Science* Online at www.sciencemag.org/cgi/content/full/293/5528/290/DC1. Included is a description of one possible reaction scheme. A key feature of this and similar schemes is the incorporation of the cis double bonds during fatty acyl chain formation by the action of the FabA dehydrase/isomerase domains.
28. D. C. Muller-Navarra, M. T. Brett, A. M. Liston, C. R. Goldman, *Nature* **403**, 74 (2000).
29. W. R. Pearson, *Methods Mol. Biol.* **132**, 185 (2000).
30. C. Bisang *et al.*, *Nature* **401**, 502 (1999).
31. We indicate the size of ORF2 as ~1.0 kb in contrast to the 0.83 kb given in the GenBank accession number U73935.1. Expression of ORF2 in *E. coli* with the ATG at position 9016 as the start codon did not produce a functional protein. In contrast, a clone including the TTG codon at position 9157 did result in production of a functional protein. Several other potential bacterial start codons (i.e., TTG or ATT) are present between positions 9157 and 9016, and it is possible that one of these codons may represent the actual start codon in *Shewanella*.
32. M. Miquel, J. Browse, *J. Biol. Chem.* **267**, 1502 (1992).
33. We thank J. Cronan (Univ. of Illinois) for the gift of *E. coli* strains, B. Shen (Univ. of CA Davis) for the help with NMR analyses, and J. Kuner (OmegaTech, Boulder, CO) for assistance with *Schizochytrium* gene sequencing. Supported in part by grants from Monsanto and the U.S. Department of Energy (grant DE-FG03-99ER20323) to J.B. and by the Agricultural Research Center, Washington State University, Pullman, WA.

5 February 2001; accepted 1 June 2001

Endothelial Apoptosis as the Primary Lesion Initiating Intestinal Radiation Damage in Mice

François Paris,[1] Zvi Fuks,[2] Anthony Kang,[1] Paola Capodieci,[3] Gloria Juan,[3] Desiree Ehleiter,[1] Adriana Haimovitz-Friedman,[2] Carlos Cordon-Cardo,[3] Richard Kolesnick[1]*

Gastrointestinal (GI) tract damage by chemotherapy or radiation limits their efficacy in cancer treatment. Radiation has been postulated to target epithelial stem cells within the crypts of Lieberkühn to initiate the lethal GI syndrome. Here, we show in mouse models that microvascular endothelial apoptosis is the primary lesion leading to stem cell dysfunction. Radiation-induced crypt damage, organ failure, and death from the GI syndrome were prevented when endothelial apoptosis was inhibited pharmacologically by intravenous basic fibroblast growth factor (bFGF) or genetically by deletion of the acid sphingomyelinase gene. Endothelial, but not crypt, cells express FGF receptor transcripts, suggesting that the endothelial lesion occurs before crypt stem cell damage in the evolution of the GI syndrome. This study provides a basis for new approaches to prevent radiation damage to the bowel.

The GI syndrome is the main toxicity associated with abdominal radiotherapy of human tumors. It consists of diarrhea, dehydration, enterobacterial infection, and in severe cases, septic shock and death (*1*). According to the prevailing hypothesis, it is caused by direct damage to a group of stem cells within the epithelial rings at positions 4 to 5 from the base of the crypts of Lieberkühn, resulting in their death (*1–3*). This etiological model is based on inference from studies of crypt regeneration after injury by using an in vivo clonogenic survival assay. Stem cell death is the critical element in the evolution of this process, because a single surviving stem cell appears sufficient for reconstitution of a crypt-villus unit (*1*). This clonogenic stem cell activity is quantified by counting regenerating crypts in histologic sections 3.5 days after irradiation (*1*). Above 8 grays (Gy), dose-dependent stem cell death leads to diminution of crypt regeneration, until the level of regeneration is insufficient to rescue the GI mucosa. In such cases, progressive denudation of the epithelium leads, by day 6 to 7 after radiation, to death of mice from the GI syndrome. Direct evaluation of stem cell function in this process is, however, not feasible because there are no markers specific for GI stem cells.

Here, we explore the alternative possibility that microvascular endothelium within the intestinal mucosa is the actual target of radiation damage, with stem cell dysfunction as a consequence. This hypothesis is supported by previous observations that (i) survival factors for endothelium [vascular endothelial growth factor (VEGF), acidic and basic FGFs, and interleukin 11 (IL-11)] protect the gut from radiation injury (*4–6*), and (ii) endothelium is a principal target for radiation injury to lung and brain (*7, 8*).

In our initial studies, we used a murine whole-body irradiation (WBR) model (*9*). The patterns of lethality and tissue damage are shown (Fig. 1) for 8- to 12-week-old C57BL/6 mice exposed to 12 to 15 Gy WBR, which exceeds the minimal dose required to kill all exposed animals within 30 days ($LD_{100/30}$). When treated with 12 or 13 Gy, 97% of mice died 10 to 13 days after irradiation (median 11 days; Fig. 1A) and displayed bone marrow aplasia and intact intestinal mucosa (Fig. 1B). Autologous marrow transplantation, performed 16 hours after 12 Gy WBR, repopulated the marrow (*10*) and rescued 90% of the mice. In contrast, exposure to 15 Gy resulted in more rapid death, with 95% of the mice dying between 6 and 8 days (mean 6.8 ± 0.99 days, median 6 days; Fig. 1A). These animals showed denudation of the intestinal crypt and villus system but had only partially damaged marrow (Fig. 1B), and could not be rescued by autologous marrow transplantation (Fig. 1A). Actuarial survival at 14 Gy differed significantly from that after 15 Gy ($P < 0.001$). At this dose, 25% of mice succumbed to death from the GI syndrome and 75% died of marrow failure ($P = 0.007$ versus death from GI syndrome at 15 Gy).

To determine whether microvascular endothelial apoptosis correlated with development of the radiation-induced GI syndrome, we evaluated tissue specimens by hematoxylin and eosin (H&E) staining, terminal dexoy transferase-mediated deoxyuridine triphosphate nick end labeling (TUNEL), and in situ labeling with annexin V (*11*), at various times after 8 to 15 Gy WBR. Previous studies have shown that radiation induces early p53-dependent (*12*) and late p53-independent (*13*) apoptotic responses in crypt epithelial cells. However, neither response affects the ability of stem cells to regenerate crypts damaged by doses ≤15 Gy (*13*) and hence do not appear to be involved in the pathogenesis of the GI syndrome. Using a published scoring system (*14*), we confirmed these observations and found a maximal epithelial apoptotic index of 40.0% at crypt position at 4 hours after 15 Gy, which decreased to 24.1% at position 5 and progressively to 4.1% at position 8. The apopto-

[1]Laboratory of Signal Transduction and [2]Department of Radiation Oncology and [3]Department of Pathology, Memorial Sloan-Kettering Cancer Center, 1275 York Avenue, New York, NY 10021, USA.

*To whom correspondence should be addressed. E-mail: r-kolesnick@ski.mskcc.org

tic index of unirradiated controls across positions 4 to 8 was 2.5% ($P < 0.05$).

Apoptosis was also observed in nonepithelial cells within the lamina propria of the villus and that surrounding crypts. Apoptosis in the lamina propria was detected by TUNEL, annexin V (Fig. 2A), and H&E staining (*15*) beginning 1 hour after 8 to 15 Gy, with maximum intensity 4 hours after irradiation. This event preceded the onset of late apoptosis in the villus columnar epithelial cell layer, which became apparent 10 hours after 15 Gy (Fig. 2A). Costaining with an antibody to CD31, which recognizes the endothelial surface marker PECAM-1 (*16*), defined these apoptotic lamina propria cells as microvascular endothelium [Fig. 2B and (*15*)]. The extent of microvascular endothelial apoptosis was quantified at 4 hours over the range of 0 to 15 Gy (Fig. 2C). In unirradiated mice, 86% of the lamina propria of the villae and crypts had no apoptotic cells; 14% had one or two apoptotic cells. At 8 Gy, the lowest dose that decreases clonogenic crypt survival (*4, 5, 17*), only 46% of crypt-villus units had no endothelial apoptosis ($P < 0.001$ versus control), whereas 29% had significant apoptosis, involving more than three apoptotic cells. As the dose increased, there was an exponential increase in the percentage of crypt-villus units with significant microvascular endothelial apoptosis [$r = 0.99$ on a semi-log plot (*10*)], and an increase in the number of apoptotic endothelial cells per affected unit (Fig. 2C). In particular, the category of >20 apoptotic cells, which represents the most extensive radiation-induced damage, occurred in only 2% of crypt-villus units at 14 Gy and increased more than 10-fold upon transition to 15 Gy. Similar rates and intensities of microvascular endothelial apoptosis were observed when villae and crypts were scored independently (*15*). These data show that there is a threshold for massive endothelial apoptosis, which correlates with the switch from death caused by marrow failure to that from the GI syndrome.

To investigate whether endothelial apoptosis is causally involved in this switch, we studied *acid sphingomyelinase* (*asmase*)$^{-/-}$ mice, which fail to generate the proapoptotic lipid ceramide in endothelium upon irradiation, and are deficient in radiation-induced endothelial apoptosis in the lung and central nervous system (*7, 8*). For controls, we used *asmase*$^{+/+}$ littermates, and mice with p53 deficiency, which abrogates the early GI crypt epithelial apoptosis (*1, 13*). The p53$^{-/-}$ mice were developed in a C57BL/6 background, so they were irradiated at 15 Gy to monitor death from the GI syndrome. The *asmase*$^{-/-}$ mice were irradiated with 16 Gy, as they were developed in an SV129/C57BL/6 background. In this background, at this dose, the cause of death switches from bone marrow failure to the GI syndrome. The apoptotic responses in tissues from p53$^{-/-}$ and *asmase*$^{-/-}$ mice after WBR are compared in Fig. 3. The p53$^{-/-}$ thymus showed little apoptosis 4 hours after irradiation, whereas the *asmase*$^{-/-}$ thymus displayed diffuse apoptosis. Consistent with previous reports (*12*), the absence of p53 caused a significant reduction in epithelial apoptosis at intestinal crypt positions 4 to 8 in p53$^{-/-}$ mice, whereas ASMase deficiency had no effect (*15*). In contrast, p53 deficiency had no effect on apoptosis in microvessels of intestinal crypt-villus units [Fig. 3 and (*15*)], whereas ASMase deficiency led to a 58% decrease in the incidence of crypt-villus units with three or more apoptotic cells and a 90% reduction in those with ≥11 apoptotic cells ($P < 0.001$; *15*). The absence of p53 did not alter the percentage of mice dying from the GI syndrome (*15*), whereas the absence of ASMase significantly reduced the percentage of mice that succumbed to the GI syndrome (15). In fact, at 16 Gy the majority of *asmase*$^{-/-}$ mice died from marrow failure rather than the GI syndrome. At this dose, median survival of *asmase*$^{-/-}$ mice was 9 days (typical of marrow failure), compared with 6 days (typical of GI syndrome) for wild-type littermates ($P < 0.001$). Similar results were obtained by using 17 Gy.

We next examined whether microvascular endothelial apoptosis was affected by the administration of basic FGF (bFGF), which has been reported to enhance murine intestinal stem cell survival and to decrease mortality after WBR (*4–6*). Intravenous (iv) injection of human recombinant bFGF into C57BL/6 mice immediately before and after irradiation with 15 Gy decreased the apoptotic microvascular damage (Fig. 2C), but did not affect apoptosis of

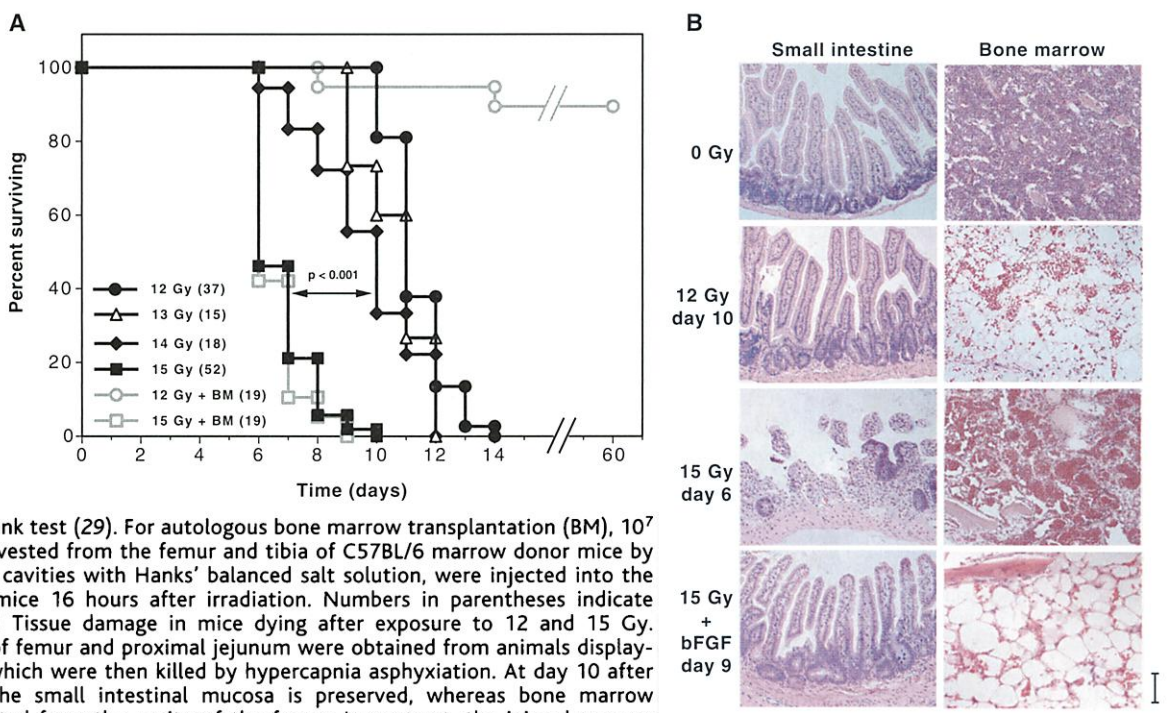

Fig. 1. Ionizing radiation induces lethal marrow and GI toxicity in C57BL/6 mice. (**A**) Actuarial survival curves of 8- to 12-week-old C57BL/6 male mice treated with 12 to 15 Gy WBR. Radiation was delivered with a ^{137}Cs irradiator (Shepherd Mark-I, model 68, SN 643) at a dose rate of 2.5 Gy/min. Actuarial survival was calculated by the product-limit Kaplan-Meier method (*28*), and *P* values were evaluated by the Mantel log-rank test (*29*). For autologous bone marrow transplantation (BM), 10^7 bone marrow cells, harvested from the femur and tibia of C57BL/6 marrow donor mice by flushing the medullary cavities with Hanks' balanced salt solution, were injected into the tail vein of recipient mice 16 hours after irradiation. Numbers in parentheses indicate animals per group. (**B**) Tissue damage in mice dying after exposure to 12 and 15 Gy. H&E-stained sections of femur and proximal jejunum were obtained from animals displaying agonal breathing, which were then killed by hypercapnia asphyxiation. At day 10 after exposure to 12 Gy, the small intestinal mucosa is preserved, whereas bone marrow elements appear depleted from the cavity of the femur. In contrast, the jejunal mucosa appeared denuded at day 6 after 15 Gy, with almost no villae or crypts apparent, whereas the marrow showed only partial damage. For studies with bFGF, mice were injected iv with 3.2 μg human recombinant bFGF in 800-ng doses delivered 30 min before, and 5, 60, and 120 min after 15 Gy. This experiment was repeated five times. Scale bar, 250 μm.

crypt epithelial cells (*15*). bFGF reduced the percentage of crypt-villus units that showed significant endothelial apoptosis (three or more apoptotic cells per unit) after 12 Gy to a value comparable to that seen at ~8 Gy without bFGF (Fig. 2C). Similarly, bFGF decreased the apoptotic damage of 15 Gy to an iso-effect observed at ~12 Gy without bFGF (Fig. 2C). H&E staining yielded similar results (*15*), and comparable protection was afforded by bFGF in the SV129/C57BL/6 background (*10*). Autopsies of animals treated with 15 Gy and iv bFGF showed that they were apt to die from marrow failure rather than the GI syndrome (Fig. 1B). Consistent with these findings, the actuarial survival of 15 Gy-irradiated mice after iv bFGF treatment increased from a mean of 6.8 ± 0.9 days (median 6 days; typical of death from GI syndrome) to 9.2 ± 1.3 days (median 9 days; typical of death caused by marrow failure; Fig. 4A). Furthermore, autologous marrow transplantation performed 16 hours after 15 Gy WBR rescued 50% of bFGF-treated mice indefinitely (Fig. 4A). The mice that died succumbed to marrow graft failure and persistent hematopoietic aplasia. Hence, all animals with successful marrow engraftment were rescued from lethal radiation damage by concomitant bFGF therapy. A similar bFGF-mediated protection of the GI tract was observed when mice were treated with whole-abdominal radiation rather than WBR (*15*).

To identify the cells responsible for the bFGF-mediated protection, we explored which mucosal cells express mRNAs for high-affinity FGF receptors (FGFRs). In situ hybridization

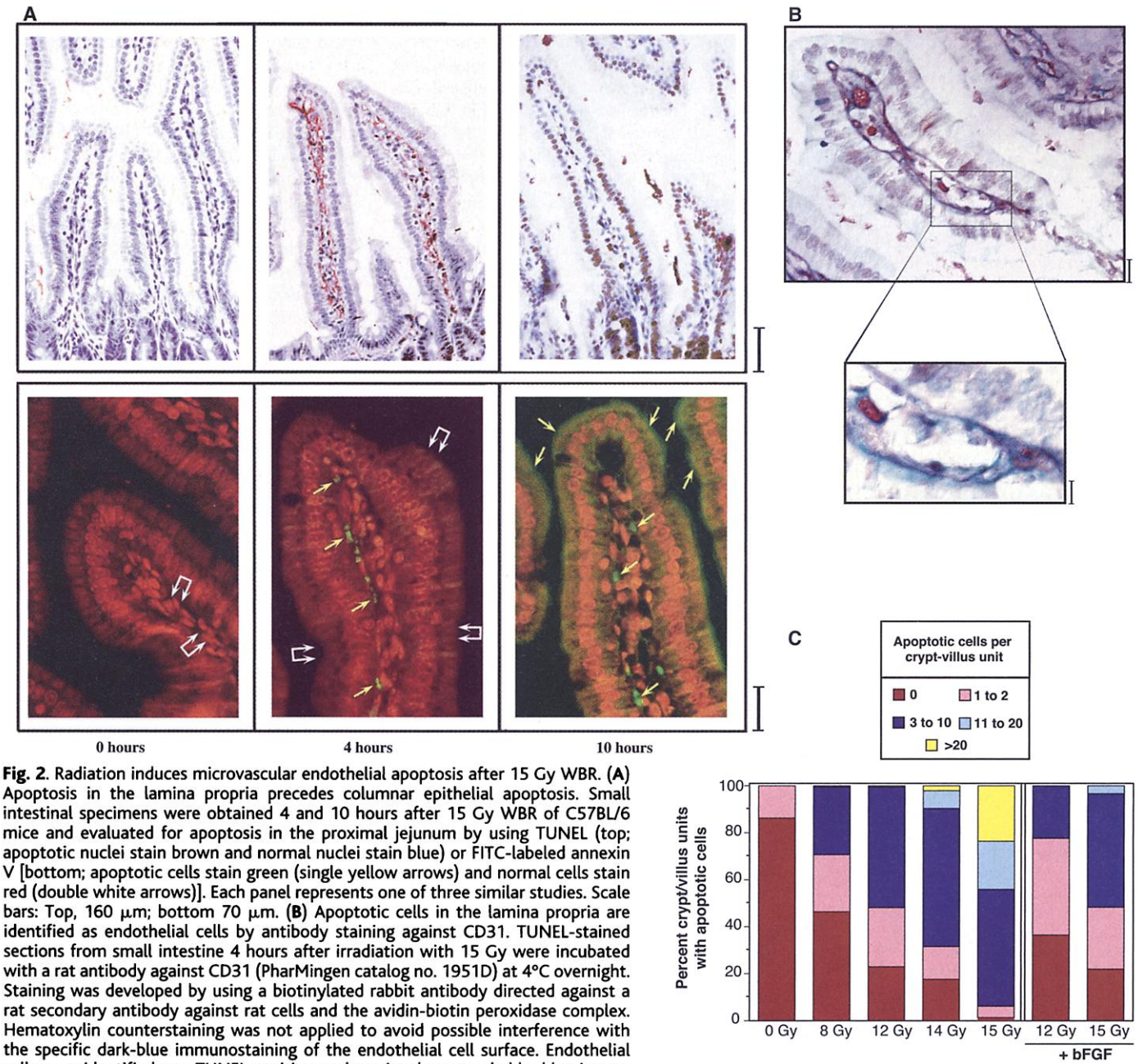

Fig. 2. Radiation induces microvascular endothelial apoptosis after 15 Gy WBR. **(A)** Apoptosis in the lamina propria precedes columnar epithelial apoptosis. Small intestinal specimens were obtained 4 and 10 hours after 15 Gy WBR of C57BL/6 mice and evaluated for apoptosis in the proximal jejunum by using TUNEL (top; apoptotic nuclei stain brown and normal nuclei stain blue) or FITC-labeled annexin V [bottom; apoptotic cells stain green (single yellow arrows) and normal cells stain red (double white arrows)]. Each panel represents one of three similar studies. Scale bars: Top, 160 μm; bottom 70 μm. **(B)** Apoptotic cells in the lamina propria are identified as endothelial cells by antibody staining against CD31. TUNEL-stained sections from small intestine 4 hours after irradiation with 15 Gy were incubated with a rat antibody against CD31 (PharMingen catalog no. 1951D) at 4°C overnight. Staining was developed by using a biotinylated rabbit antibody directed against a rat secondary antibody against rat cells and the avidin-biotin peroxidase complex. Hematoxylin counterstaining was not applied to avoid possible interference with the specific dark-blue immunostaining of the endothelial cell surface. Endothelial cells were identified as a TUNEL-positive nuclear signal surrounded by blue immunohistochemical staining for CD31. This experiment represents one of three similar studies. Scale bars: Top, 50 μm; bottom, 15 μm. **(C)** Frequency histograms of apoptotic cells in the lamina propria of irradiated crypt-villus units. Small intestinal specimens were obtained 4 hours after 0 to 15 Gy WBR and stained for apoptosis by TUNEL. Apoptotic cells were scored in the lamina propria of 400 units per point. Data represent mean scores from three experiments. Crypt-villus units were scored as having >20 apoptotic cells when the exact number of apoptotic nuclei could not be determined because groups of adjacent nuclei coalesced (see Fig. 3, left bottom).

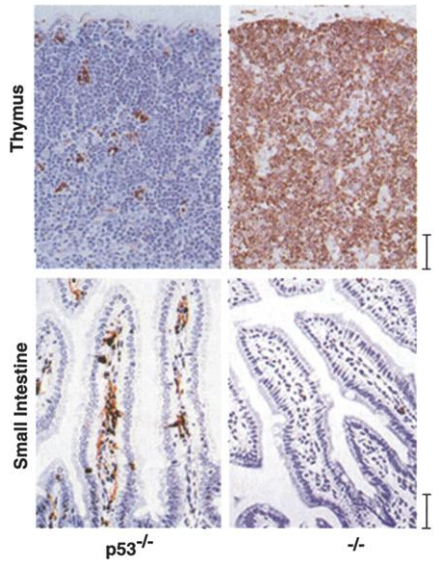

Fig. 3. ASMase deficiency but not p53 deficiency protects against radiation-induced microvascular apoptosis and death from the GI syndrome. Thymic and small intestine tissue from 15 Gy-irradiated $p53^{-/-}$ C57BL/6 mice or 16 Gy-irradiated $asmase^{-/-}$ SV129/C57BL/6 mice were stained by TUNEL. This experiment represents one of three similar studies. Scale bars: Top, 200 μm; bottom, 140 μm.

with probes specific for FGFRs detected cytoplasmic staining in selected subpopulations of the gut mucosa. We used digoxigenin-labeled probes to identify FGFR-1 to FGFR-4 transcripts and either digoxigenin-AP (Fig. 4B, top) or digoxigenin-rhodamine-FITC (Fig. 4B, middle and bottom) as readout systems (*18*). Both techniques are highly sensitive to detection of small amounts of transcripts (*19–21*). An added advantage of labeling with digoxigenin-AP is that it permits concomitant evaluation of endothelium by double-staining for FGFR transcripts and CD31 (Fig. 4B, upper left panel). The most intense FGFR transcript staining observed with digoxigenin-AP–labeling was in cells in the lamina propria and adventitia, which were identified by double-staining with antibody against CD31 as endothelium, whereas Paneth cells displayed intermediate-intensity FGFR staining (Fig. 4B, upper left). Studies using the digoxigenin-rhodamine-FITC method confirmed that FGFR-1 to FGFR-4 mRNA transcripts are expressed in endothelial cells, but not in epithelial cells of the crypts or villae, except for Paneth cells (Fig. 4B, middle and bottom). It should be noted that FGFRs were not up-regulated in epithelial cells at any time from 1 to 12 hours after irradiation.

We also investigated the distribution of injected bFGF within the intestinal mucosa. Consistent with published data (*4*), immunohistochemical studies using a monoclonal antibody against human bFGF detected a reticular pattern of bFGF deposits within the lamina propria 15 min after treatment, but not within or adjacent to crypts (*15*). The lack of ligand and receptor in the crypts precludes stem cells as the direct target of bFGF protection.

Basic FGF protected C57BL/6 mice from death caused by the GI syndrome with WBR doses up to 18 Gy. At 18 Gy, however, five out of five mice died at 6.4 ± 1.1 days, despite bFGF pretreatment. TUNEL staining of intestinal specimens obtained 4 hours after 18 Gy showed extensive endothelial apoptosis in only 10.7% of bFGF-treated mice (≥11 per crypt-villus unit; not significantly different from 14 Gy without bFGF, Fig. 2C), compared with 69% in mice receiving 18 Gy alone ($P < 0.001$). Nonetheless, all five animals that died after 18 Gy plus bFGF displayed the histological pattern typical for death from GI syndrome ($P < 0.01$ versus 14 Gy without bFGF). A similar switch to death from the GI syndrome was observed in $asmase^{-/-}$ mice receiving 18

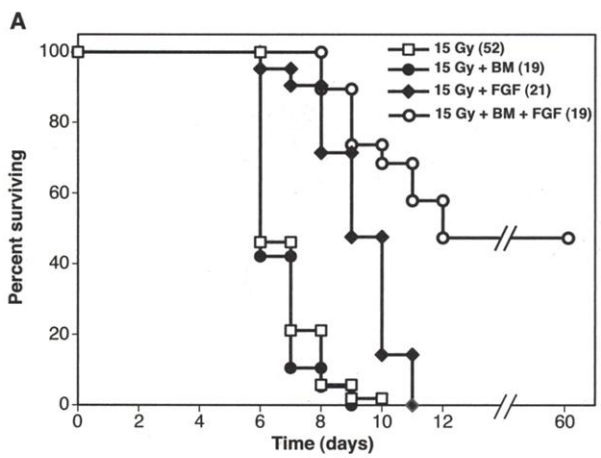

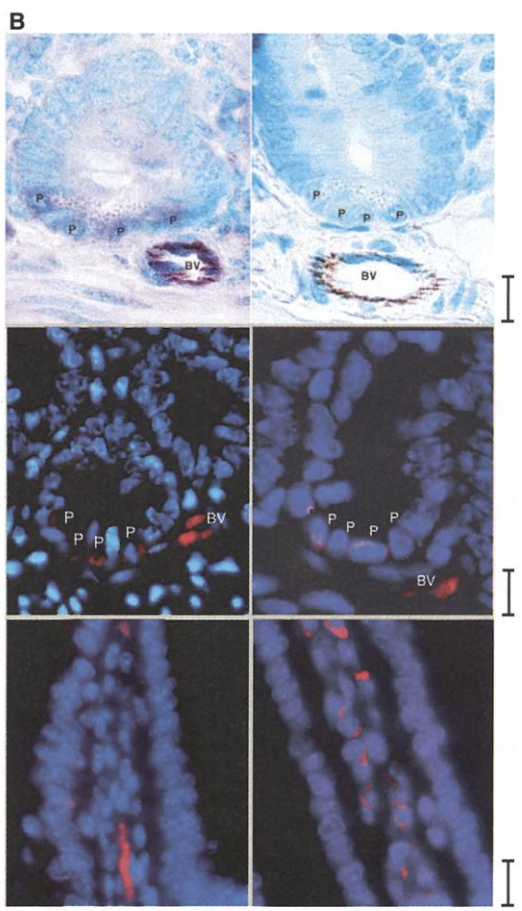

Fig. 4. The endothelial survival factor bFGF protects against radiation-induced microvascular apoptosis and death from the GI syndrome. (**A**) Treatment with both bFGF and bone marrow rescues mice from radiation-induced death. Actuarial survival curves of 15 Gy-irradiated C57BL/6 mice treated with bFGF and/or bone marrow transplantation (BM) (as in Fig. 1A) were calculated by the product-limit Kaplan-Meier method. Numbers in parentheses indicate animals per group. Scale bar, 30 μm. (**B**) Endothelial and Paneth cells, but not other epithelial crypt or villus cells, express *FGFR* transcripts. Sections of proximal jejunum from C57BL/6 mice were hybridized in situ with digoxigenin-AP-labeled antisense *FGFR-4* (upper left), or sense *FGFR-4* (upper right) as negative control, and costained for endothelial cell PECAM-1 by using an antibody against CD31, as in Fig. 2B. *FGFR-4* transcripts are represented by the bright blue granular cytoplasmic staining, and endothelial cell membranes are identified by the strong brown stain. Paneth cells (P) at the crypt base are identified by large white cytoplasmic secretory granules, and confirmed by immunohistochemical staining for lysozyme. Note strong *FGFR* hybridization in endothelial cells of a blood vessel (BV) in the adventitia, less intense staining in Paneth cells (P), and lack of staining in other crypt cells. Similar results were obtained upon assessing expression of *FGFRs 1* to *3* with digoxigenin-AP (*30*), and with digoxigenin-rhodamine (middle and bottom). Upon hybridization with digoxigenin-rhodamine labeled antisense *FGFRs 1* to *4*, *FGFR* transcripts are identified by the bright red staining, whereas DAPI counterstaining is bright blue. Antisense probes for *FGFR-4* (middle left) and *FGFR-2* (middle right) show positive staining in Paneth cells (P) and microvascular endothelial cells (BV), but not in other crypt cells. BV were identified as blood vessels by the green fluorescence emitted by paraffin-fixed erythrocytes within the core of these structures by using a green filter. Lower left and right panels show that cells in the laminapropria of villae, but not epithelial cells, hybridize with antisense *FGFR-1* and *FGFR-3*, respectively. Erythrocytes were identified adjacent to the red-fluorescing cells in the villae lamina propria, indicating that *FGFR*-expressing cells are endothelial cells. Two hundred villae and crypts were scored for each *FGFR* transcript. Scale bars, 30 μm.

Gy without bFGF (REF *10*). These data indicate that although ASMase-mediated microvascular endothelial apoptosis is the prevailing mechanism for induction of the GI syndrome at WBR doses <18 Gy, an alternative mechanism, perhaps involving direct damage to stem cells, is engaged by higher radiation doses.

Our studies provide evidence that radiation damage to GI stem cell clonogens, regarded as the critical lesion in the pathogenesis of the GI syndrome, is a consequence of extensive microvascular injury. The vulnerability of the microvascular endothelium to stress appears related to the abundance of ASMase in endothelium (20 times as much as in other cell types) (*22*) and to its preferential trafficking to the plasma membrane. ASMase exists in lysosomal and secretory isoforms (*23*), both produced by posttranscriptional processing of a single gene product. The secretory isoform targets the plasma membrane, may reside in caveolar microdomains (*24*), and is also found extracellularly at the cell surface (*23, 24*). Further, inflammatory cytokines, such as interleukin-1β and interferon-γ, increase ASMase secretion threefold (*22*), indicating that under stress, endothelial cells mobilize excess amounts of membrane-targeted ASMase.

The specific sensitivity of microvascular versus large vessel endothelium to stress may be associated with bFGF distribution within vascular basement membranes. Although bFGF is ubiquitously expressed in basement membranes of large and intermediate size blood vessels, microvascular basement membranes have minimal or absent bFGF deposits (*25*). Ultrastructural studies indicate that capillaries represent the most radiation-sensitive sections of the vascular system (*26*). Because basement membrane–bound bFGF protects endothelial cells against radiation-induced cell death in vitro (*27*), its lack of expression in microvascular basement membranes may render this section of the vascular system highly sensitive to ASMase-mediated apoptosis.

Finally, our studies suggest that small molecules, such as bFGF, may improve the therapeutic ratio during WBR for leukemia, and abdominal radiation therapy for gastrointestinal, genitourinary, and gynecological tumors. A potential for therapeutic gain would likely be limited to patients in whom tissue typing demonstrates tumors to be insensitive to bFGF. Further, we propose that a requirement for ASMase-mediated ceramide generation in induction of microvascular endothelial apoptosis, and its inhibition by bFGF, represent a generic model for evolution of and protection against normal tissue damage after environmental, chemical, or toxic stress.

References and Notes

1. C. S. Potten, *Int. J. Radiat. Biol.* **58**, 925 (1990).
2. C. S. Potten *et al.*, *Int. J. Exp. Pathol.* **78**, 219 (1997).
3. C. Booth, C. S. Potten, *J. Clin. Invest.* **105**, 1493 (2000).
4. C. W. Houchen *et al.*, *Am. J. Physiol.* **276**, G249 (1999).
5. P. Okunieff *et al.*, *Radiat. Res.* **150**, 204 (1998).
6. W. B. Khan *et al.*, *Radiat. Res.* **148**, 248 (1997).
7. P. Santana *et al.*, *Cell* **86**, 189 (1996).
8. L. A. Pena *et al.*, *Cancer Res.* **60**, 321 (2000).
9. P. Okunieff *et al.*, *Br. J. Cancer Suppl.* **27**, S105 (1996).
10. F. Paris , R. Kolesnick, unpublished data.
11. Late-stage and early-stage apoptosis were assessed by TUNEL (*7*) and by in situ labeling with annexin V [A. L. Bronckers *et al.*, *Histochem. Cell Biol.* **113**, 293 (2000)]. To identify endothelial cells, we immunostained tissue with a rat monoclonal antibody against CD31 as in (*16*), except that we used a biotinylated rabbit antibody directed against a rat secondary antibody (1:100 dilution) and omitted the counterstaining. For annexin V staining, we injected mice iv with 0.5 mg of annexin V–FITC (Sigma, St Louis, MO) and killed mice 30 min later by hypercapnia asphyxiation. Tissue sections were counterstained with propidium iodide and scored by fluorescence microscopy.
12. C. S. Potten, H. K. Grant, *Br. J. Cancer* **78**, 993 (1998).
13. A. J. Merritt *et al.*, *Oncogene* **14**, 2759 (1997).
14. A. J. Merritt, L. S. Jones, C. S. Potten, in *Techniques in Apoptosis* T. G. Cotter, S. J. Martin, Eds. (Portland Press, London, 1996), pp. 269–299.
15. Supplementary material is available on *Science* Online at www.sciencemag.org/cgi/content/full/293/5528/293/DC1
16. A. Haimovitz-Friedman *et al.*, *J. Exp. Med.* **186**, 1831 (1997).
17. N. H. Terry, E. L. Travis, *Int. J. Radiat. Oncol. Biol. Phys.* **17**, 569 (1989).
18. Mouse *FGFR* cDNA sequences were incorporated into pBluescript SK^{50} plasmids, and included *FGFR 1b, 1c, 2b, 2c, 3b, 3c,* and *FGFR-4* [D.M.Omitz *et al.*, *J. Biol. Chem.* **271**, 15292 (1996)]. *FGFR-1* and *FGFR-3* probes were generated by polymerase chain reaction using specific primers to produce T3 promoter-tailed DNA fragments. These were subsequently used as templates to transcribe the sense and antisense riboprobe with T3 polymerase. *FGFR-2* and *FGFR-4* probes were transcribed from the pBluescript SK^{50} plasmids. Recombinant plasmid (1 μg) was linearized by Bgl II and Nhe I, or Nco I and Not I, respectively, to generate sense and antisense transcripts. Riboprobes were generated with T7 and T3 polymerases for 2 hours at 37°C in 1× transcription buffer (Boehringer Mannheim, Indianapolis) containing 20 U of RNase inhibitor; 1 mmol/liter each of ATP, GTP, and CTP; 6.5 mmol/liter of UTP; and 3.5 mmol/liter of digoxigenin-UTP. In situ hybridization was carried out by using deparaffinized tissue sections rinsed in water and phosphate-buffered saline for 10 min. Slides were digested in prewarmed citrate buffer for 5 min in a microwave. Prehybridization was performed for 30 min at 45°C in 50% deionized formamide and 2× SSC. For hybridization, 10 pmol/liter of digoxigenin-labeled riboprobe was added to 50 μl hybridization buffer [50% deionized formamide (v/v), 10% dextran sulfate, 2× SSC, 1% SDS, and 0.25 mg/ml of herring sperm DNA]. After overnight incubation at 45°C, slides were washed twice for 20 min in prewarmed 2× SSC at 42°C, followed by two washes in prewarmed 1× SSC at 42°C for 20 min. Slides were then incubated in normal sheep serum diluted in buffer 1 (2 M Tris HCl, 5 M NaCl, pH 7.5). In some experiments, slides were incubated in the same buffer with antibody against digoxigenin-AP (Boehringer Mannheim, Indianapolis, IN) at a dilution of 1:500 for 1 hour at room temperature. Visualization of hybridized transcripts was accomplished by nitroblue tetrazolium 5-bromo-4-chloro-3-indolylphosphate. Slides were counterstained with methyl green and mounted. In other experiments, hybridization was at 42°C and slides were incubated with antibody against digoxigenin-rhodamine (Boehringer Mannheim) at a dilution of 1:200 for 1 hour at 37°C, in the dark. Slides were counterstained in 4,6-diamino-2-phenylindole (DAPI), mounted, and examined by using a fluorescent microscope (Olympus VX40) with blue and red filters.
19. P. Capodieci *et al.*, *Diagn. Mol. Pathol.* **7**, 69 (1998).
20. C. Magi-Galluzzi *et al.*, *Lab. Invest.* **76**, 37 (1997).
21. H. Fahimi, E. Baumgart, *J. Histochem. Cytochem.* **47**, 1219 (1999).
22. S. Marathe *et al.*, *J. Biol. Chem.* **273**, 4081 (1998).
23. S. L. Schissel *et al.*, *J. Biol. Chem.* **273**, 18250 (1998).
24. R. T. Dobrowsky, V. R. Gazula, *Methods Enzymol.* **311**, 184 (2000).
25. C. Cordon-Cardo *et al.*, *Lab. Invest.* **63**, 832 (1990).
26. H. S. Reinhold, L. F. Fajardo, J. W. Hopewell, *Adv. Radiat. Biol.* **14**, 177 (1990).
27. Z. Fuks *et al.*, *Eur. J. Cancer* **28A**, 725 (1992).
28. E. L. Kaplan, P. Meyer, *J. Am. Stat. Assoc.* **53**, 447 (1958).
29. N. Mantel, *Cancer Chemother. Rep.* **50**, 163 (1966).
30. C. Cordon-Cardo, P. Capodieci, unpublished data.

31. We thank S. Jio for outstanding technical support and M. Goldfarb for the *FGFR* cDNAs. These studies were supported by grants CA85704 (R.K.) and CA52462 (Z.F.), and a Fellowship from the Association pour la Recherche sur le Cancer (F.P.).

26 February 2001; accepted 25 May 2001

Molecular Evolution of Protein Atomic Composition

Peggy Baudouin-Cornu,[1] Yolande Surdin-Kerjan,[1] Philippe Marlière,[2] Dominique Thomas[1]*

Living organisms encounter various growth conditions in their habitats, raising the question of whether ecological fluctuations could alter biological macromolecules. The advent of complete genome sequences and the characterization of whole metabolic pathways allowed us to search for such ecological imprints. Significant correlations between atomic composition and metabolic function were found in sulfur- and carbon-assimilatory enzymes, which appear depleted in sulfur and carbon, respectively, in both the bacterium *Escherichia coli* and the eukaryote *Saccharomyces cerevisiae*. In addition to genetic instructions, genomic data thus also provide paleontological records of environmental nutrient availability and of metabolic costs.

A widely accepted principle is that protein evolution is mainly determined by constraints on activity, specificity, folding, and stability (*1–4*). But other constraints may come into play, in particular nutritional constraints, which have thus far received little scrutiny. Indeed, the elements used in the construction of proteins are not only funneled through metabolic pathways but are also subject to geochemical cycles at the surface of Earth.